Journal of Applied Polymer Science

Synthesis of Novel Polyaniline/MgO Composite for Enhanced Adsorption of Reactive Dye

K. Pandiselvi, A. Manikumar, S. Thambidurai
Department of Industrial Chemistry, School of Chemical Sciences, Alagappa University, Karaikudi 630003, Tamil Nadu, India
Correspondence to: S. Thambidurai (E-mail: sthambi01@yahoo.co.in)

ABSTRACT: In this investigation, the porous structure of polyaniline/MgO (PANI/MgO) composites has been successfully synthesized by in-situ oxidative polymerization method. The as-prepared materials were characterized by Ultraviolet–visible absorption spectroscopy, Fourier transform infrared spectroscopy, X-ray diffraction, and scanning electron microscopy. The obtained composites, for the first time, are used as an adsorbent for the removal of the sulfonated anionic dye reactive orange 16 (RO) from aqueous solution. The equilibrium adsorption isotherms of RO on the PANI/MgO composites were analyzed by Langmuir and Freundlich models, suggesting that the Langmuir model provides the better correlation of the experimental data and maximum adsorption capacity was found to be 558.4 mg g^{-1}. In addition, adsorption kinetics was followed by both pseudo-first-order and pseudo-second-order, but the latter model matches the results much better than the former one. © 2013 Wiley Periodicals, Inc. J. Appl. Polym. Sci. **2014**, *131*, 40210.

KEYWORDS: adsorption; composites; kinetics; dyes/pigments; porous materials

Received 23 September 2013; accepted 19 November 2013
DOI: 10.1002/app.40210

INTRODUCTION

The extensive use of dyes in dye-manufacturing industries creates significant problems due to the discharged of colored waste water. The presence of very small amounts of dyes in water is visible and affects the quality of water.[1] Hence, color removal from dye effluents is one of the main concerns of society today. To date, a variety of methods have been developed for the removal of dye pollutants from colored effluents, such as biological treatment, coagulation/flocculation, ozone treatment, chemical oxidation, membrane filtration, ion exchange, photocatalytic degradation, and adsorption,[2] each of these has specific advantages and disadvantages. The survey of literature reveals that adsorption technology with no chemical degradation is a effective method for color removal due to its economy, simplicity of design, ease of operation and insensitivity to toxic substances, but it application is limited by the high price of some adsorbents and the large amounts of waste water normally involved. Therefore, searching for novel alternative adsorbents with high adsorptive capacity and low producing cost should be of considerable significance for practical application of adsorption.[3]

Recently, some investigators directed their research toward application of polyaniline (PANI) for environmental remediation. PANI is considered to be one of the most promising classes of organic conducting polymers due to their well-defined electrochemistry, easy protonation reversibility, excellent redox recyclability,[4] good environmental stability,[5] and variety of nanostructured morphologies.[6] For example, Mahanta et al.[7] used PANI emeraldine salt (ES) for the removal of sulfonated dyes. Ai et al.[8] reported that the PANI microspheres possess potential efficiency to removal methyl orange from aqueous solution. However, the use of PANI powders could be limited by the polymer surface area. To overcome these limitations, using nanostructured PANI or incorporating functional materials, inorganic metal oxide nanoparticles, heteropolyacidic anions, etc.[9,10] The principle is based on the chelating properties attributed to the electron-donating groups (large number of amine and imine functional groups) on the PANI polymers.[11] Zang et al.[12] reported nitrogen doped cuprous oxide exhibits good optical and electrical properties.

In this regard, inorganic nanomaterials due to their surface area, corner defect sites, and thus a large fraction of atoms are available for chemical reaction. Several researchers have shown use of nanocrystalline metal oxides like MgO, c-Al_2O_3, MnO_2, and Zn-Al layered double hydroxides and oxides as adsorbents for the removal of pollutants.[13–16] Among these materials, porous metal oxides, in particular MgO/$Mg(OH)_2$, have promising applications as adsorbents in water treatment because of their low production cost, minimal environmental impact and essential for plant, animal, and human life. Accordingly, porous MgO adsorbents template with different structure-directing agents are extensively used as effective sorbents for reactive and vat dyes in waste water.[17,18] Furthermore, as the pH of zero

© 2013 Wiley Periodicals, Inc.

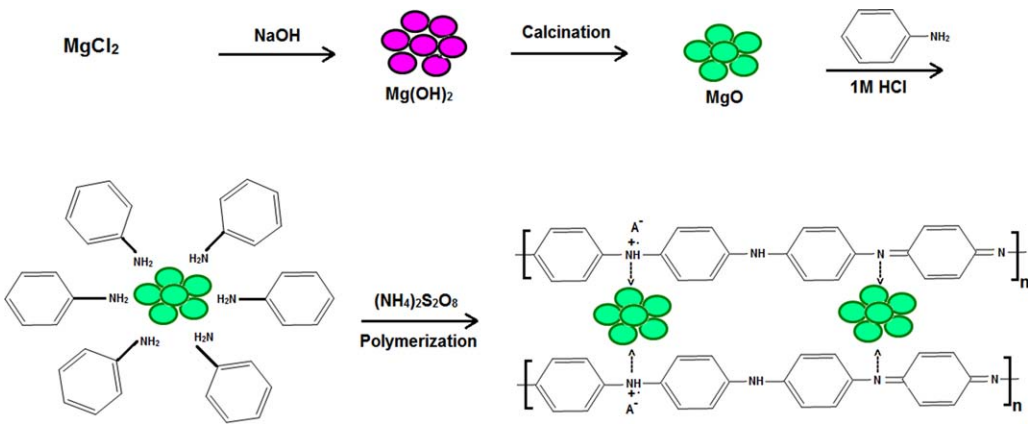

Scheme 1. Schematic process of the formation of the PANI/MgO composites. [Color figure can be viewed in the online issue, which is available at wileyonlinelibrary.com.]

point charge (pHzpc) of MgO is 12.4,[19] it is a suitable adsorbent for the adsorption of anions due to its favorable electrostatic attraction mechanism. Up to date, few researchers have been made to Fe_2O_3/PANI,[20] SiO_2/PANI,[21] and PANI/CS[22] for the removal of organic dyes from aqueous solution. To our knowledge, a novel polymer composite that composes of PANI enwrapping nanosized MgO nanoparticles (PANI/MgO) synthesis and relation to its physicochemical structure has not yet been reported. Hence, the objective of this work was to develop simple and cost effective method for the removal of reactive orange 16 (RO) dye from aqueous solution using PANI/MgO composites. The effects of some important parameters such as pH, exposure time, initial dye concentration, and adsorbent dosage on the adsorption capacity of PANI/MgO have been investigated. The advantages of using PANI/MgO composites onto RO dye is higher adsorption capacities than previous reported pristine PANI and MgO nanoparticles. This result is explained that porous PANI/MgO composites may have a higher surface area and larger number of binding sites available to interact more with anionic dye RO occurs.

EXPERIMENTAL

Materials

Monomer aniline (Merk) was distilled under reduced pressure and stored in dark below 4°C. Ammonium peroxydisulfate (APS), hydrochloric acid, magnesium chloride ($MgCl_2$ $6H_2O$), and sodium hydroxide were obtained from S.D. Fine Chemicals Ltd., and used without any further purification. Analytical grade RO (formula: C_{20} H_{17} N_3 Na_2 O_{11} S_3, molecular weight: 617.54 g mol^{-1}, λmax: 494 nm) was used to prepare stock solutions of 500 mg L^{-1}, which were further diluted to the required concentrations before use. RO is a reactive dye bearing an azo group as chromophore and a sulfato-ethylsulfone as the reactive group. Double distilled water was used to prepare all the solutions.

Preparation of MgO Nanoparticles

The MgO nanoparticles were synthesized via the method reported by Moussavi and Mahmoudi[23] with a slight modification. The procedure was as follows: 5 g of $MgCl_2.6H_2O$ was dissolved in 100 mL distilled water in 500 mL beaker, into which 100 mL of 1*M* NaOH solution was added slowly and rapidly stirred for 4 h to generate the magnesium hydroxide precipitates. Then, it was allowed to settle for 24 h to obtain white precipitate was washed several times with distilled water, dried overnight in an oven at 60°C and finally calcined at 400°C for 2 h in a muffle furnace to get MgO nanoparticles.

Synthesis of PANI

PANI was synthesized by chemical oxidation coupled with polymerization in the presence of HCl using ammonium persulfate [$(NH_4)_2S_2O_8$] as an oxidant. One mL of aniline monomer was dissolved in 1*M* HCl (80 mL) solution and stirred for 15 min. Then 2.49 g of APS was dissolved in 20 mL of 1*M* HCl was added drop wise into the above solution and continuously stirred for 2 h at 4°C. During the addition, the solution became green color indicating the formation of PANI. The resulting product was collected by filtering and washing with deionized water and methanol, and dried in air oven at 60°C for 24 h.

Preparation of PANI/MgO Composites

PANI/MgO composite were prepared by the same way of PANI in the presence of MgO nanoparticles. Aniline (1 mL) was dissolved in 1*M* HCl to form aniline solution. Synthesized MgO nanoparticles were dispersed into aqueous 1*M* HCl solution via sonication for 10 min to obtain uniform suspension, which was added to the aniline solution to keep the MgO nanoparticles suspended in the solution. To this reaction mixture, 2.49 g of APS $(NH_4)_2S_2O_8$ in 1*M* HCl, which act as oxidant was added slowly with continuous stirring at 4°C. After complete addition of the oxidizing agent, the reaction mixture was kept under stirring for 2 h. The greenish black precipitate of the polymer was recovered by vacuum filtration and washed with deionized water. Finally, the obtained composite (PANI/MgO) was dried in an oven at 80°C for 24 h to achieve a constant weight. Preparation process of PANI/MgO composites is shown in Scheme 1. Several composites were synthesized with different wt % of MgO (0.5, 1.5, 2.5, and 4 wt %) with respect to the monomer. The corresponding composites were designed as PANI/$MgO_{0.5}$, PANI/$MgO_{1.5}$, PANI/$MgO_{2.5}$, and PANI/MgO_4.

Adsorption Experiments

Adsorption experiments were conducted at contact time, initial dye concentrations, adsorbent dosages, and various solution pH

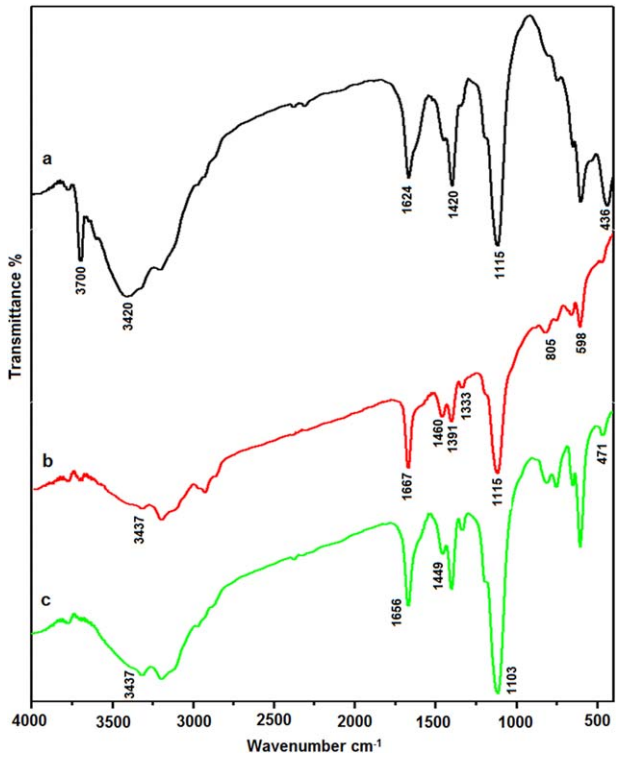

Figure 1. FT-IR spectra of (a) MgO, (b) PANI, and (c) PANI/MgO. [Color figure can be viewed in the online issue, which is available at wileyonlinelibrary.com.]

values in batch mode. The solution pH was adjusted to a given value by adding either 0.1 mol L^{-1} HCl or NaOH solution before adsorption experiment. Adsorption experiments were conducted in a conical flask containing given volume of dye solution and required dosage of adsorbent were stirred on a magnetic stirrer with agitation speed of 100 rpm at room temperature. During this process, samples were collected from the reaction beaker at different time intervals, and the residual concentration of dye was determined by UV–vis absorption spectroscopy at 495 nm. The equilibrium adsorption capacity q_e was determined by the following equation:

$$q_e = \frac{C_o - C_e}{M} V \quad (1)$$

where C_o and C_e are the concentrations of RO in aqueous solution at initial time and at equilibrium time, respectively (mg L^{-1}); V is the volume of RO solution (L); M is the mass of adsorbent (mg). The dye removal efficiency was calculated using the following equation:

$$\text{Removal efficiency}\,(\%) = \frac{C_o - C_e}{C_o} \times 100 \quad (2)$$

Instrumentation

The morphology of the samples was characterized by high resolution scanning electron microscopy (HRSEM-FEI Quanta FEG 200 and HRTEM-CM200 model) with an accelerating voltage of 30.0 kV. Powder X-ray diffraction (XRD) study was carried out using PHILIPS-1710 X-ray diffractometer. Cu Ka radiation ($k = 1.5418$ A°) was used with a scan rate of 0.02 V in the 2θ range of 10–80°. Fourier transform infrared spectroscopy (FT-IR) spectra of the samples were measured on a PerkinElmer 2000 Model spectrophotometer at a resolution of 2 cm^{-1} using the KBr technique. Ultraviolet–visible (UV–vis) absorption spectra were measured on a SHIMADZU (UV-2401pc). The pH measurement were carried out with a digital pH-meter (ELICO LI120) equipped with a glass electrode.

RESULTS AND DISCUSSION

Characterizations

FT-IR spectrum is used to analyze the functional groups, nature of bonding, and the chemical structure of compounds. The FT-IR spectra of the MgO nanoparticles, PANI, and PANI/MgO composites are presented in Figure 1. As shown in Figure 1(a), the broad vibration band at 3420 cm^{-1} is associated with the OH stretching vibrations of water molecules (physical adsorbed molecular water), while those at 1624 cm^{-1} are associated with their bending mode. The band at 1420 cm^{-1} is characteristic absorption peak of CO_3^{2-}, whereas the band at 1115 cm^{-1} is attributed to the asymmetric stretching vibrations CO group. The band at 3700 cm^{-1} is associated with the vibration of magnesium hydroxide. Due to its alkaline and high activity after calcinations treatment in this study, MgO sample easily absorbed the CO_2 and H_2O in the air. The wide, strong absorption band at 436 cm^{-1} is the stretching vibration of MgO.[24] From the spectrum of Figure 1(b), the PANI exhibits characteristic peaks around 3437 cm^{-1} is attributed to N—H stretching mode,[25] the C═N and C═C stretching of quinoid and benzenoid units occur at 1667 and 1460 cm^{-1}, respectively. In addition, the bands at 1391 and 1333 cm^{-1} are assigned to the C—N stretching of benzenoid unit while the band at 1115 cm^{-1} is due to "electronic-like band" and is considered to be a measure of the degree of delocalization of electrons, is a characteristic peak of the doped PANI.[26] The band at 805 cm^{-1} is associated with C—C and C—H for benzenoid ring.[27] The FT-IR spectrum of MgO impregnated PANI composites [Figure 1(c)] represents the same characteristic peaks with the PANI. However, the corresponding peaks are shifted to the lower wave numbers, besides their intensities are changed after the MgO nanoparticles addition. The peaks of the PANI around 1667, 1460, and 1115 cm^{-1} are shifted to 1656, 1449, and 1103 cm^{-1}, respectively. Theses shifts of characteristic peaks of the PANI may be the result of the interactions between the PANI chains and MgO nanoparticles, which affect the electron densities and bond energies of the PANI.[28,29] The shifting of lower wave numbers may be shows the increasing the electron density of PANI chains. Furthermore, the sharp band at 471 cm^{-1} can be assigned to MgO stretching vibrations. This indicates that the PANI/MgO composites exhibit both the characteristic band of PANI and MgO, which confirms the presence of both components in the composites.

The absorption spectrum of the MgO nanoparticles [Figure 2(a)] exhibits three absorption peaks around 338, 499, and 666 nm, which is the characteristics of MgO nanoparticles. As reported previously by some researchers ES form of PANI show usually three characteristic absorption bands at 300–330, 400–430, and 500–700 nm.[30] Similarly, we observed the free

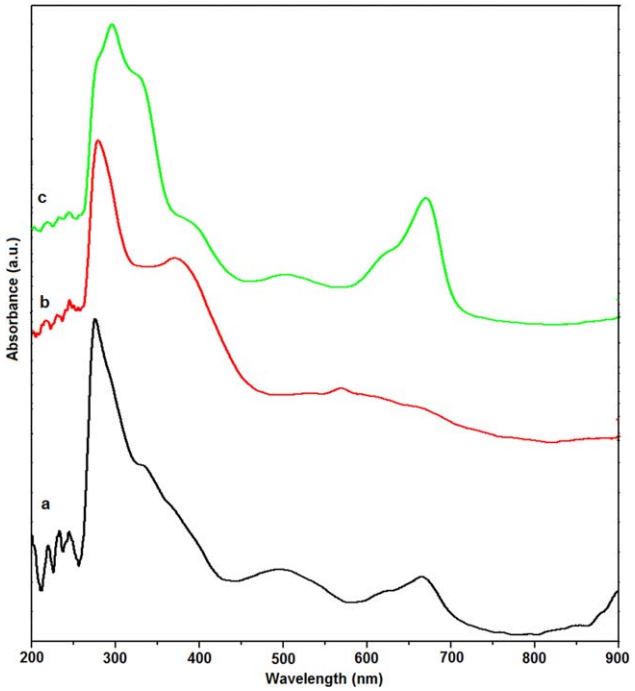

Figure 2. UV–vis spectra of (a) MgO, (b) PANI, and (c) PANI/MgO. [Color figure can be viewed in the online issue, which is available at wileyonlinelibrary.com.]

PANI has three characteristic peaks at 280, 37 (small shoulder), and broad absorbance band around 619 nm. On comparison to free PANI, the absorbance bands at 280 and 371 nm have red shifted and move to higher wavelength of 310 and 400 nm, respectively in PANI/MgO might due to the interaction increase with decreasing PANI content in the composite. The similar red-shift has been also observed in SnO_2/PANI composites.[31] In addition to these peaks, we observed new features at 510 and 670 nm could be due to the MgO nanoparticles that have chemically interacted with PANI. This result indicates that the PANI molecules might form a partial bond with MgO nanoparticles.

The XRD patterns of MgO nanoparticles, PANI, and PANI/MgO composites were shown in Figure 3. The MgO nanoparticles (curve a) shows, all the diffraction peaks matched well with the face centered cubic structure of MgO (JCPDS No. 87–0653). The major peaks at 2θ values of 37.1°, 43.0°, 62.4°, 74.8°, and 78.6° can be indexed to the lattice planes of (111), (200), (220), (311), and (222), respectively. Furthermore, no characteristic peaks from other crystalline impurities were detected by XRD, suggesting that the product was pure magnesium oxide. In addition, crystallite size was calculated using Scherrer formula[32] for MgO nanoparticles was fund to be 54.6 nm. In the pattern of pure PANI [Figure 3(b)], the peak centered at $2\theta = 20°$ is ascribed to a periodicity parallel to the polymer chain, while the peak at $2\theta = 25°$ is due to the periodicity perpendicular to the polymer chain.[33] The former peak represents the characteristic distance between the planes of benzene rings in adjacent chains or the close contact interchain distance,[34] while the latter peak maybe assigned to the scattering from PANI chains at interplanar spacing[35,36] and indicates that the PANI has also some degree of crystallinity. From this Figure 3(c), PANI/MgO composites show the peaks corresponding to PANI and no additional characteristic peaks of MgO nanoparticles were appeared. However, it is observed that small defined MgO peaks at $2\theta = 36°$ and 42° corresponding to the planes of (111) and (200), respectively. This result may be attributed to low MgO/Aniline molar ratio and polymerization degree of the PANI. The similar behavior was observed by Eskizeybek et al. and Divya and Sangaranareyanan[37,38]

FESEM measurements were carried out in order to deduce the morphology of the synthesized MgO, PANI, and PANI/MgO composites are shown in Figure 4. It can be seen that MgO nanoparticles [Figure 4(a)] synthesized by a precipitation process are irregular rod-like structure, with few aggregates due to their high surface energy. Similar results were observed by Mageshwari and Sathyamoorthy.[39] From Figure 4(b), it is observed that the pure PANI reveals presence of the rod-like aggregate structure. This may perhaps be attributed to the secondary growth of the PANI structures during the early stage of polymerization. The same observations can be found in the literature.[40,41] However, Figure 4(c) shows the porous nature of PANI/MgO composites confirming the difference in the particle sizes of the two materials, which is also reflected from UV–vis spectra [Figure 2(c)]. A tremendous change in the morphology of the composite occurs due to the presence of Mg^{2+} makes the growth rate of PANI greatly increased, which improve the

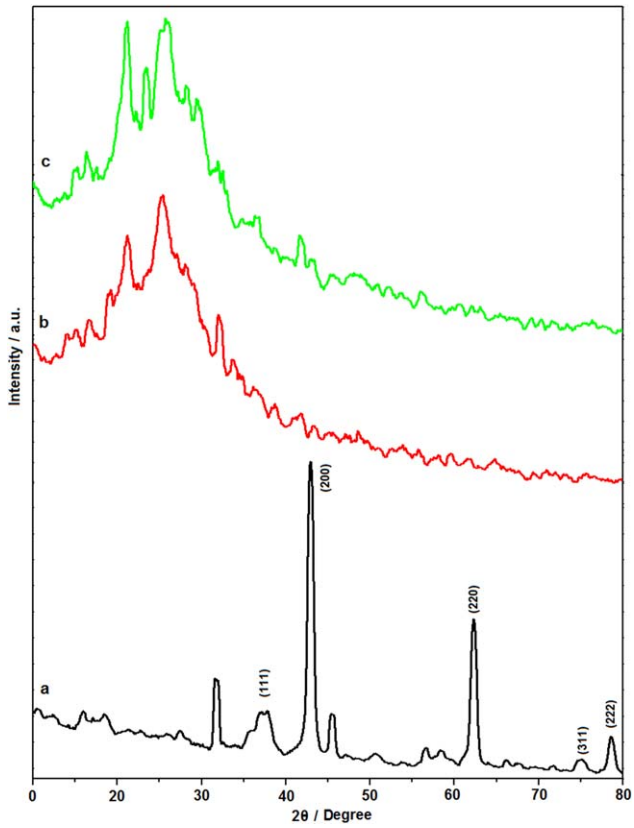

Figure 3. XRD patterns of (a) MgO, (b) PANI, and (c) PANI/MgO. [Color figure can be viewed in the online issue, which is available at wileyonlinelibrary.com.]

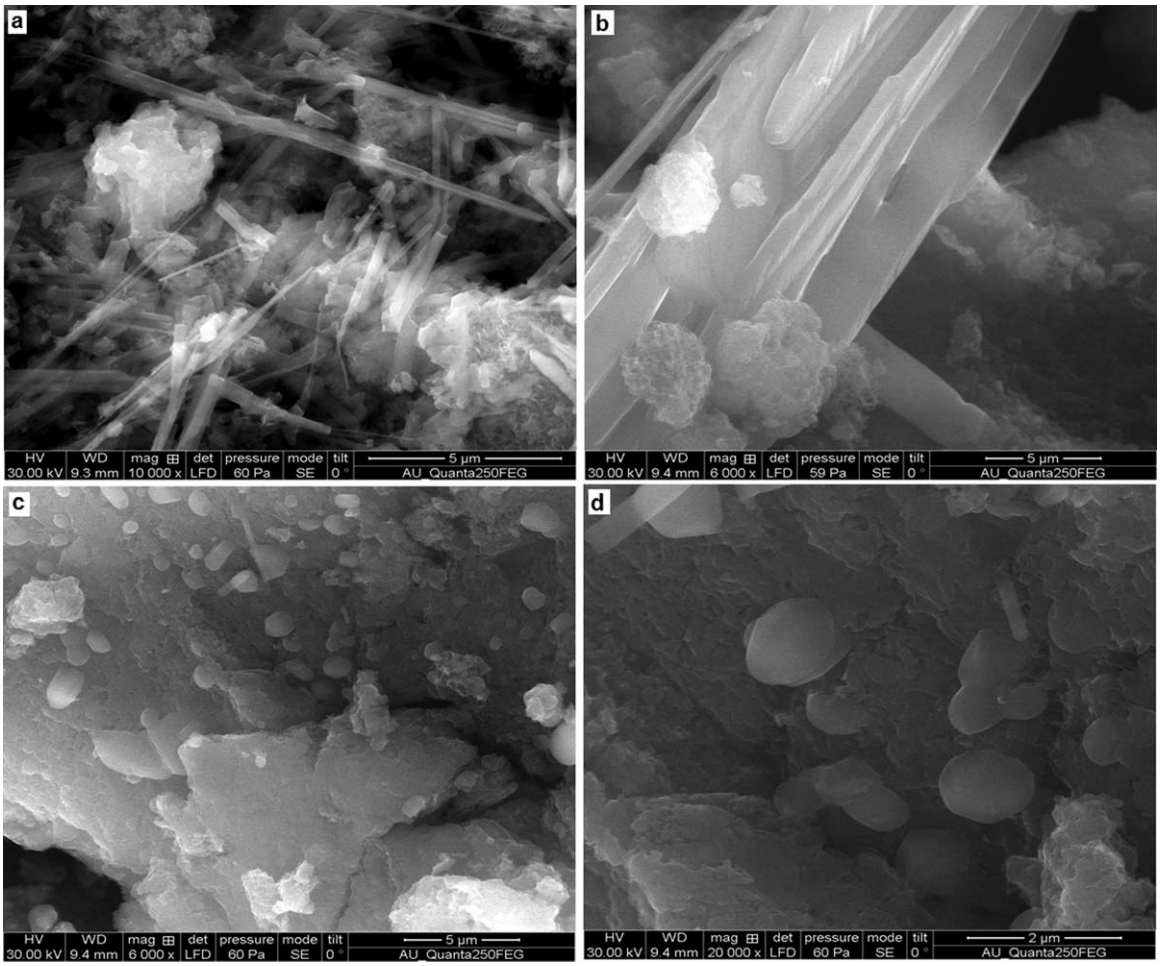

Figure 4. SEM images of (a) MgO, (b) PANI, and (c, d) 5 and 2 μm of PANI/MgO.

density of nucleation. Consequently, a transition metal ion such as Mg^{2+} has multiple doping positions and may bind to several nitrogen sites in PANI chains by coordination.[42] Furthermore, the absence of any MgO nanorods or flake indicated that reduces the particle size and increase the surface area/internal space of the composites. This sphere like particles ensures a high reaction rate which enables greater adsorption of dye molecules from waste water (environmental applications). At high magnification [Figure 4(c)], we clearly observed that these spherical particles are residing on the surface of PANI matrix.

Adsorption Properties

Comparison of RO Adsorption with Different Adsorbents. Adsorption capacity of RO as a function of contact time with different adsorbents, namely PANI, MgO, and different wt % of MgO nanoparticles incorporated PANI composites are shown in Figure 5. It is obvious from these results that the adsorption capacity of PANI/MgO composites was higher than that of both PANI and MgO, which may be explained by a synergy between PANI and MgO. The enhanced adsorption capacities of PANI/MgO composites can be explained the following reasons: (1) Introduction of MgO nanoparticles onto PANI provided many active sites (hydroxyl and amino groups) on the surface of PANI/MgO composite. (2) The PANI/MgO composites have much larger surface areas and macroporous or mesoporous structures compared with PANI and MgO; this has been proved by the result of SEM analysis. (3) MgO nanoparticles embedded in polymer matrix expanded adsorption capacity due to electrostatic attraction between the protonated amino groups of PANI and anionic dye ions affected the adsorption.[43] Further the experimental conditions, intermolecular reactions, and hydrogen bonding between adsorbate and adsorbent played important roles in the removal of RO. The effect of MgO ratio on the adsorption properties of the synthesized PANI/MgO composites are also presented in Figure 5. The dye removal efficiency increased with the increase of MgO ratio. This result can be explained by the greater number of adsorption sites for dye molecules made available at greater MgO nanoparticles.[44,45] Increasing the MgO ratio up to 4% did not affect the removal of RO dye. Therefore, we selected the optimum ratio of MgO nanoparticles (4%) with PANI composites was used as adsorbent for dye removal in the following study. The saturation adsorption capacities of PANI, MgO, and PANI/MgO_4 were measured as 443, 512, and 788 mg g^{-1}, respectively. At the same time, it can be seen 5 min of adsorption time, adsorption capacity of RO onto PANI, MgO and PANI/MgO reached sharply to 335, 456, and 740 mg g^{-1}, respectively. However, with further increase in adsorption time from 5 to 40 min,

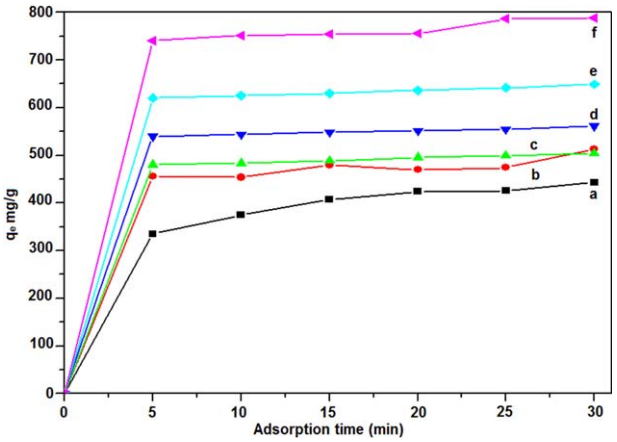

Figure 5. Removal efficiency of RO dye (100 mg L^{-1}) with time in presence of 0.1 g L^{-1} PANI (a), MgO (b), PANI/$MgO_{0.5}$ (c), PANI/$MgO_{1.5}$ (d), PANI/$MgO_{2.5}$ (e), and PANI/MgO_4 (f) at pH 7. [Color figure can be viewed in the online issue, which is available at wileyonlinelibrary.com.]

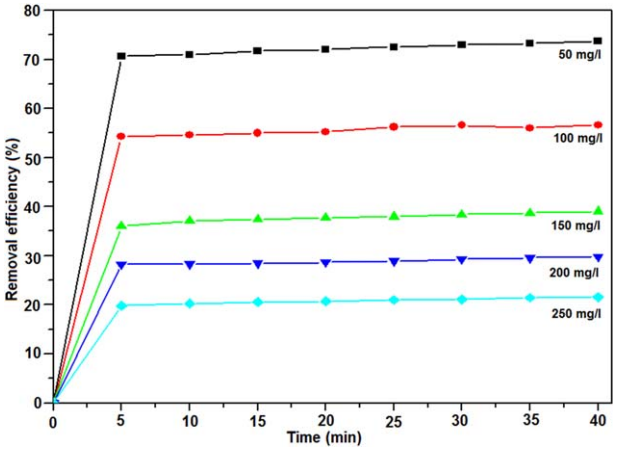

Figure 6. Effect of initial dye concentration varied from (50–250 mg L^{-1}) with time in the presence of PANI/MgO under the experimental conditions: adsorbent dose; 0.1 g L^{-1}, pH 7. [Color figure can be viewed in the online issue, which is available at wileyonlinelibrary.com.]

corresponding q_e of RO onto three adsorbents increased only by 108, 56, and 48 mg g^{-1}, indicating that the adsorption equilibriums had been achieved. It indicated that the adsorption capacity of PANI/MgO toward RO was better than both activated carbon and natural material in previous research.[46,47]

Effect of Contact Time and Initial Dye Concentration. The adsorption of RO on PANI/MgO composites at different initial dye concentrations (50–250 mg L^{-1}), pH (7) and adsorbent dosage (0.1 g L^{-1}) was analyzed as a function of contact time to depict the equilibrium time. The effect of initial dye concentration and time on the adsorption of RO by PANI/MgO composites is shown in Figure 6. Amounts of RO adsorbed increased rapidly within the first 5 min and remained almost unchanged after 40 min, indicating an equilibrium state. The increased activity at initial stage could be due to the availability of more adsorption site on PANI/MgO composite surface, and gradual occupancy of these sites reduced the reaction rate and the adsorption becomes less efficient. It is observed that the removal efficiency of low concentration (50 mg L^{-1} was achieved 73%), could be due to the faster movement of dye into the activated sites of composites. However, in higher concentration the removal rate was decreased (250 mg L^{-1} was 21.5%) due to saturation of the adsorption sites. The shorter the contact time in an adsorption system, the lower would be the capital and operational costs for real-world applications. The contact time obtained in this study for equilibrium adsorption is shorter than most of the reported values for dye adsorption onto other adsorbents.[23,48]

Effect of Adsorbent Dosage. The effect of adsorbent dosage (varied from 0.1 to 0.5 g L^{-1}) on the percentage removal of 100 mg L^{-1} RO solution at pH 7.0 is shown in Figure 7(a). The percentage removal of RO from the solution increased from 72.3 to 92.7% as the adsorbent dosage increased from 0.1 to 0.5 g L^{-1}. Increased adsorbent concentration implies a greater surface area of PANI/MgO composites and, consequently, a greater number of binding sites. However, the adsorbent doses 0.4 and 0.5 g L^{-1} had not significantly increased the removal efficiency

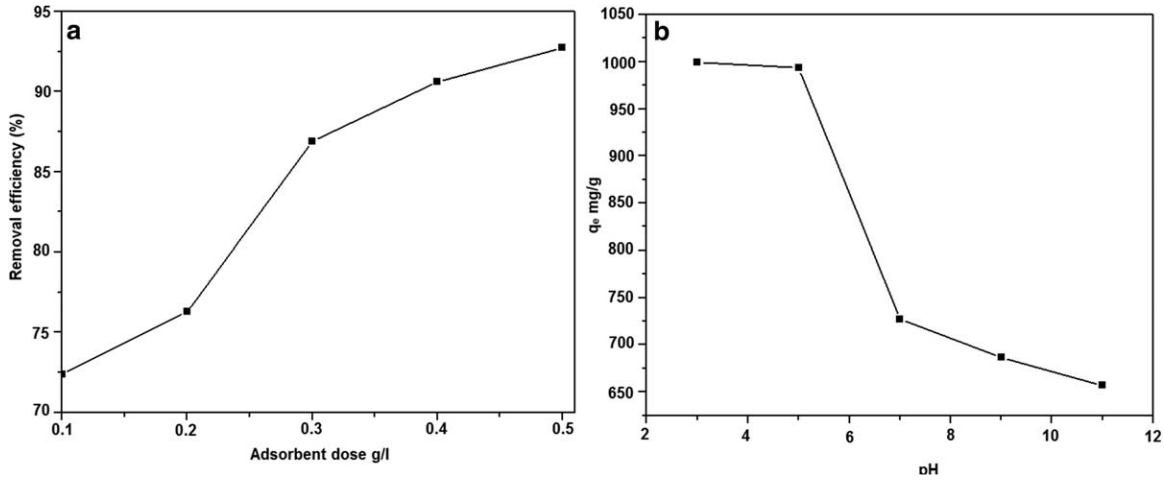

Figure 7. (a) Effect of adsorbent dosage varied from (0.1–0.5 g L^{-1}) on RO removal by PANI/MgO (dye concentration; 100 mg L^{-1}, pH 7). (b) Effect of pH varied from (3–11) 0n RO removal by PANI/Mgo (dye concentration; 100 mg L^{-1}, dosage concentration; 0.1 g L^{-1}).

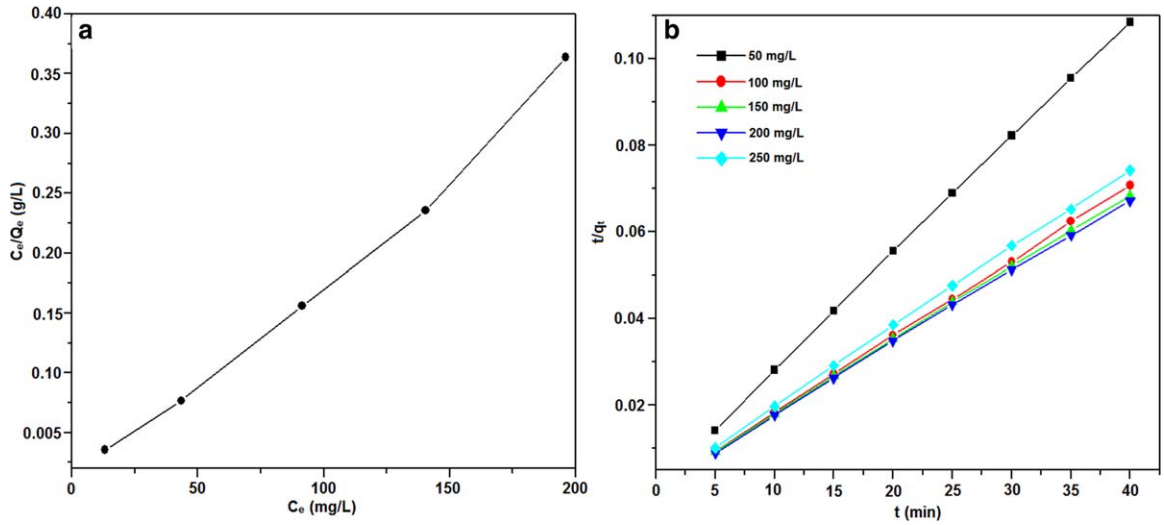

Figure 8. (a) Langmuir isotherm and (b) pseudo-second-order kinetic model for the adsorption RO onto PANI/MgO composites. [Color figure can be viewed in the online issue, which is available at wileyonlinelibrary.com.]

and adsorption equilibrium rate. The limited removal rate at high adsorbent dosage could be due to the concentration gradient between the PANI/MgO composites and dye solution. From an economic point of view, the adsorbent dosage in the present all experiments was 0.1 g L^{-1}.

Effect of pH. The influence of pH is an important parameter that determined the adsorption capacity (q_e) onto PANI/MgO. The experiments were carried out in pH range 3–11 and the results are illustrated in Figure 7(b). After 40 min of adsorption, RO adsorption capacity (q_e) sharply increased to 999 and 993 mg g^{-1} with corresponding pH 3 and 5. Then decreased from 727 to 686 mg g^{-1} with further increasing pH from 7 to 9. With further increase in the initial solution pH at 11, q_e of RO decreased evidently to 656 mg g^{-1}. Therefore, optimum pH range from RO adsorption onto PANI/MgO was 3–5. This result can be explained by the fact that more protons were available to protonate amine groups to form —NH_3 group in pH 3.9,[7] thereby enhancing the electrostatic attraction between negatively charged dye anions and positively charged surface of PANI/MgO. However, Moussavi and Mahmoudi reported, P.Z.C of MgO 12.4 was reached at pH 6.0.[23] Therefore, the dye anions can be bound by electrostatic attractions to both PANI and MgO when the ambient pH was <5.0. Additionally, the increase in the solution pH beyond 7.0 resulted in the deprotonation of amine groups and de-doping of composite. Moreover, the presence of excess OH^- ions may compete with the dye anions. The results clearly bring out the importance of PANI as well as the doping level of MgO in its dye adsorption characteristics.

Adsorption Isotherms

The equilibrium adsorption isotherm model, which is the number of mg adsorbed per gram of adsorbent (q_e) versus the equilibrium concentration of adsorbate, is fundamental in describing the interactive behavior between adsorbate and adsorbent. The analysis of isotherm data is important for predicting the adsorption capacity of the adsorbent, which is one of the main parameters required for the design of an adsorption system. The adsorption process is normally described by Langmuir and Freundlich isotherms, which are defined by the following equations:

$$\frac{C_e}{q_e} = \frac{1}{K_L q_{\max}} + \frac{C_e}{q_{\max}} \quad (3)$$

$$\log q_e = \log K_F + \frac{1}{n}\log C_e \quad (4)$$

where q_e (mg g^{-1}) is the amount of RO sorbed at equilibrium, $q_{\max}$ (mg g^{-1}) the theoretical maximum monolayer sorption, C_e (mg L^{-1}) the equibrium concentration of RO in solution and K_F, n, and K_L are empirical constants. Langmuir and Freundlich parameters are calculated from eqs. (3) and (4), the correlation coefficient for the Langmuir model was appreciably larger than that for the Freundlich model ($R^2L = 0.991$, $R^2F = 0.662$). The best-fit Langmuir parameters are $q_m = 558.4$ mg g^{-1},

Table I. Comparison of Adsorption Capacities of Various Sorbents to Anionic Reactive Dyes

Adsorbent	Dyes	Adsorption capacity (mg g^{-1})	References
PANI microspheres	Methyl orange	154.56	49
PANI/CS	Remazol brilient blue R	303.03	50
PANI/EPS	RO	293.2	51
CS-ZnO/PANI	RO	476.2	52
MgO	Methyl orange	370.0	53
MgO	Reactive blue 19	166.7	23
MgO	Levafix Fast Red CA	92.16	54
MgO	Reactive blue 19	250	17
PANI/MgO	**RO**	**558.4**	**This work**

Table II. The Pseudo-First, Pseudo-Second-Order Kinetic Model Constants for the Adsorption of the RO Dye onto PANI/MgO Composite, for Different Initial Dye Concentrations, pH 7, Adsorbent Dose 0.1 g L^{-1}, and Temperature 30°C

			Pseudo-first-order			Pseudo-second-order		
S. no.	C_o (mg L^{-1})	q_e exp (mg g^{-1})	k_1 (1/min)	q_1, cal (mg g^{-1})	R^2	k_2 (g mg^{-1} min^{-1})	q_2, cal (mg g^{-1})	R^2
1	50	361.197	0.00233	350.75	0.988	0.00301	370.9	0.999
2	100	555.66	0.00267	539.51	0.879	0.00208	570.0	0.999
3	150	567.162	0.00408	540.75	0.943	0.00118	591.8	0.999
4	200	578.139	0.00316	557.18	0.975	0.00123	601.0	0.999
5	250	520.465	0.00447	493.17	0.972	0.00111	546.5	0.999

$K_L = 0.05596$, and Freundlich parameters are $K_F = 276.69$, $1/n = 1.4125$. This result indicated that the experimental date fitted well with Langmuir iostherm for RO [Figure 8(a)], suggesting the monolayer coverage of dyes on the adsorbent surface. The Freundlich model showed very poor fit for the experimental data in RO dye and hence the corresponding isotherm figure was not shown here. Based on the Langmuir isotherm model, the maximum adsorption capacity of PANI/MgO composites was much higher than that of other adsorbents had been reported in the previous literatures (Table I), suggesting that the as-prepared composite possesses more reactive surfaces due to the presence of high concentrations of edge/corner sites and other defects. Furthermore, the essential feature of the Langmuir isotherm can be expressed in terms of a dimensionless constant separation factor (R_L) given by the following (5):

$$R_L = \frac{1}{1 + K_L C_o} \tag{5}$$

R_L values within the range $0 < R_L < 1$ indicate a favourable adsorption. In this study, the calculated RL value is 0.1516, thus the adsorption of RO onto PANI/MgO composites is favorable. From an environmental perspective, obtaining a relatively high capacity and short contact time required, present the prepared prepared new PANI/MgO composites as an attractive and promising adsorbent for reactive dye removal in practical applications.

Adsorption Kinetics

Kinetics is important for adsorption studies because it can predict the rate at which a pollutant is removed from aqueous solutions and provides valuable data for understanding the mechanism of sorption reactions. To investigate the mechanism of the dye sorption onto PANI/MgO composites, pseudo-first-order and pseudo-second-order kinetic models are given by:

$$\log(q_e - q_t) = \log q_e - \frac{K_1}{2.303} t \tag{6}$$

$$\frac{t}{q_t} = \frac{1}{K_2 q_e^2} + \frac{t}{q_e} \tag{7}$$

where q_e and q_t are the adsorption capacities for adsorbent (mg g^{-1}) at equilibrium and at any time t, respectively; k_1 and k_2 is the rate constant of pseudo-first-order and pseudo-second-order kinetic model (1/min). The calculated kinetic parameters for RO sorption by PANI/MgO composites are given in Table II. It seems that, of the two kinetic equations tested, the pseudo-second-order model best described the kinetic date for RO sorption by PANI/MgO, based on the correlation coefficient R^2. Pseudo-second-order kinetic model for RO adsorption by PANI/MgO composite is shown in Figure 8(b). Several earlier researchers have also shown that pseudo-second-order model fits well in describing the adsorption process.[55–58] The pseudo-second model suggests that the adsorption depends on the adsorbate as well as adsorbent and involves chemisorptions process in addition to physisorption.

CONCLUSIONS

In summary, a novel PANI/MgO composite was successfully prepared and used as an effective adsorbent to remove the RO dye from aqueous solution. The effects of contact time, dye concentration, adsorbent dosage, and initial pH on the removal of RO were investigated separately through batch experiments. The adsorption process of RO onto PANI/MgO composites follows the pseudo-second-order kinetic model and the experimental results fitted well with Langmuir isotherm model, which suggest that the adsorption process is monolayer chemisorptions. The monolayer adsorption capacity of PANI/MgO composites obtained was 558.4 mg g^{-1}, which was much higher than that of many other previously reported adsorbents. The as-prepared PANI/MgO composites are non-toxic material and can be made in a simple and cost-effective way for waste water treatment. Therefore, this method is promising potential of this adsorbent material for dye removal.

REFERENCES

1. Banat, I. M.; Nigam, P.; Singh, D.; Marchant, R. *Bioresour. Technol.* **1996**, *58*, 217.
2. Garg, V. K.; Gupta, R.; Yadav, A. B.; Kumar, R. *Bioresour. Technol.* **2003**, *89*, 121.
3. Bi, B.; Xu, L.; Xu, B.; Liu, X. *Appl. Clay Sci.* **2011**, *54*, 242.
4. Wu, M. S.; Wen, T. C.; Gopalan, A. *Mater. Chem. Phys.* **2002**, *74*, 58.
5. Camalet, J. L.; Lacroix, J. C.; Aeiyach, S.; Chane-ching, K.; Lacaze, P. C. *Synth. Met.* **1998**, *93*, 133.
6. Stejskal, J.; Sapurina, I.; Trchova, M. *Prog. Polym. Sci.* **2010**, *35*, 1420.

7. Mahanta, D.; Madras, G.; Radhakrishnan, S.; Patil. S. *J. Phys. Chem. B* **2008**, *112*, 10153.
8. Ai, L.; Jiang, J.; Zhang, R. *Synth. Met.* **2010**, *160*, 762.
9. Liu, X. X.; Bian, L. J.; Zhang, L.; Zhang, L. J. *J. Solid State Electrochem.* **2007**, *11*, 1279.
10. Prastomo, N.; Ayad, M. M.; Kawamura, G.; Matsuda, A. *J. Ceram. Soc. Jpn.* **2011**, *119*, 342.
11. Tang, L.; Wu, T.; Kan, J. *Synth. Met.* **2009**, *159*, 1644.
12. Zang, Z.; Nakamura, A.; Temmyo, J. *Mater. Lett.* **2013**, *92*, 188.
13. Hu, J.; Song, Z.; Chen, L.; Yang, H.; Li, J.; Richards, R. *J. Chem. Eng. Data.* **2010**, *55*, 3742.
14. Cai, W.; Jiaguo, Y.; Jaroniec, M. *J. Mater. Chem.* **2010**, *20*, 4587.
15. Chen, H.; He, J. *J. Phys. Chem. C* **2008**, *112*, 17540.
16. Zhou, J.; Yang, S.; Jiaguo, Y.; Shu, Z. *J. Hazard. Mater.* **2011**, *192*, 1114.
17. Venkatesh, T. G.; Viswanath, R.; Arthoba Nayak, Y.; Chethan, B. K. *Chem. Eng. J* **2012**, 198–199, 1.
18. Li, X.; Xia, W.; He, G.; Zheng, W.; Yu, N.; Tan, M. *Colloids Surf. A* **2012**, *408*, 79.
19. Crittenden, J. C.; Trussell, R. R.; Hand, D. W.; Howe, K. J.; Tchobanoglous, G. Water Treatment: Principals and Design, 2nd ed.; MWH, Wiley, **2005**.
20. Janaki, V.; Vijayaraghavan, K.; Ramasamy, A. K.; Lee, K. J.; Oh, B. T.; Kamala kannan, S. *J. Hazard. Mater.* **2012**, *241*, 110.
21. Ayad, M. M.; El-Nasr, A. A.; Stejskal, J.; *J. Ind. Eng. Chem.* **2012**,*18*, 1964.
22. Janaki, V.; Oh, B. T.; Shanthi, K.; Lee, K. J.; Ramasmy, A. K.; *Kamala-Kannan. Synth. Met.* **2012**, *162*, 947.
23. Moussavi, G.; Mahmoudi, M. *J. Hazard. Mater.* **2009**, *168*, 806.
24. Hsu, J. P.; Nacu, A. *Colloids Surf. A* **2005**, *262*, 220.
25. Zheng, W.; Angelopoulos, M.; Epstein, A. J.; MacDiarmid, A. G. *Macromolecules* **1997**, *30*, 2953.
26. Quillard, S.; Louarn, G.; Lefrant, S.; MacDiarmid, A.G. *Phys. Rev. B* **1994**, *50*, 12496.
27. Zhang, L. X.; Liu, P.; Su, Z. X. *Polym. Degrad. Stab.* **2006**, *91*, 2213.
28. Somani, P. R.; marimuthu, R.; Mulik, U. P.; Sainkar, S. R.; Amelnerkar, D. P. *Synth. Met.* **1999**, *106*, 45.
29. Niu, Z.; Yang, Z.; Hu, Z.; Lu, Y.; Han, C. C. *Adv. Funct. Mater.* **2003**, *13*, 949.
30. Wang, X.; Li, Y.; Zhao, Y.; Liu, J.; Saide, T.; Feng, W. *Synth. Met.* **2010**, *160*, 2008.
31. Schnitzler, D. C.; Meruvia, M. S.; Hümelgen, I. A.; Zarbin, A. J. G. *Chem. Mater.* **2003**, *15*, 4658.
32. Inan, S.; Altas, Y. *Sep. Sci. Technol.* **2010**, *45*, 269.
33. Chen, J.; Xu, Y.; Zheng, Y.; Dai, L.; Wu, H.; Chen, J.; Xu, Y.; Zheng, Y.; Dai, L.; Wu, H. *Compt. Rend. Chim.* **2008**, *11*, 84.
34. Zhang, L.; Long, Y.; Chen, Z.; Wan, M. *Adv. Funct. Mater.* **2004**, *14*, 693.
35. Min, S.; Wang, F.; Han, Y. *J. Mater. Sci.* **2007**, *42*, 9966.
36. Feng, W.; Sun, E.; Fujii, A.; Wu, H.; Nihara, K.; Yoshino, K. *Bull. Chem. Soc. Jpn.* **2000**, *73*, 2627.
37. Eskizeybek, V.; Sari, F.; Gulce, H.; Gulce, A.; Avci, A. *Appl. Catal., B* **2012**, 119– 120, 197.
38. Divya, V.; Sangaranareyanan, M. V. *Eur. Polym. J.* **2012**, *48*, 560.
39. Mageshwari, K.; *Sathyamoorthy. Trans. Indian Ins. Met.* **2012**, *65*, 49.
40. Reddy, K. R.; Sin, B. C.; Yoo, C. H.; Sohn, D.; Lee, Y. *J. Colloid Interface Sci.* **2009**, *340*, 160.
41. Jing, X.; Wang, Y.; Wu, D.; She, L.; Guo, Y. *J. Polym. Sci. Part A: Polym. Chem.* **2006**, *44*, 1014.
42. Yang, C. M.; Chen, C. Y. *Synth. Met.* **2005**, *153*, 133.
43. Luo, X. G.; Zhang, L. N. *J. Hazard. Mater.* **2009**, *171*, 340.
44. Li, X.; John, V. T.; Zhan, J.; He, G.; He, J.; Spinu, L. *Langmuir* **2011**, *27*, 6252.
45. Li, X.; John, V. T.; He, G.; Zhan, J.; Tan, G.; McPherson, G.; Bose, A.; Sarkar, J. *Langmuir* **2009**, *25*, 7586.
46. Dotto, G. L.; Pinto, L. A. A. *J. Hazard. Mater.* **2011**, *187*, 164.
47. Nemr, A. E.; Abdelwaha, O.; El-Sikaily, A.; Khaled, A. *J. Hazard. Mater.* **2009**, *161*, 102.
48. Zhu, H. Y.; Jiang, R.; Xiao, L. *Appl. Clay Sci.* **2010**, *48*, 522.
49. Aia, L.; Jiang, J.; Zhang, R. *Synth. Met.* **2010**, *160*, 762.
50. Janaki, V.; Oh, B. T.; Shanthi, K.; Lee, K. j.; Ramasamy, A. K.; Kamala-kannan, S. *Synth. Met.* **2012**, *162*, 974.
51. Janaki, V.; Vijayaraghavan, K.; Ramasamy, A. K.; Lee, K. J.; Oh, B. T.; Kamala kannan, S. *J. Hazard. Mater.* **2012**, 241–242, 110.
52. Pandiselvi, K.; Thambidurai, S. *Colloids Surf. B* **2013**, *108*, 229.
53. Li, X.; Xiao, W.; He, G.; Zheng, W.; Yu, N.; Tan, M. *Colloids Surf. A* **2012**, *408*, 79.
54. Nga, N. K.; Hong, P. T. T.; Lam, T. D.; Huy, T. Q. *J. Colloid Interface Sci.* **2013**, *398*, 210.
55. Nga, N. K.; Hong, P. T. T.; Lam, T. D.; Huy, T. Q. *J. Colloid Interface Sci.* **2013**, *398*, 210.
56. Dotto, G. L.; Pinto, L. A. A. *J. Hazard. Mater.* **2011**, *187*, 164.
57. Lunhong, A.; n Huang, H.; Chen, Z.; Wei, X.; Jiang, J. *Chem. Eng. J.* **2010**, *156*, 243.
58. Saravanabhavan, S.; Sreeram, K. J.; Rao, J. R.; Nair, B. U. *J. Chem. Technol. Biotechnol.* **2007**, *82*, 407.